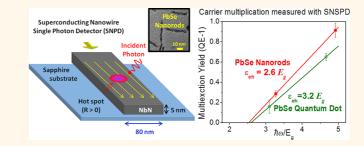# Multiexciton Dynamics in Infrared-Emitting Colloidal Nanostructures Probed by a Superconducting Nanowire Single-Photon Detector

Richard L. Sandberg,[†] Lazaro A. Padilha,[†] Muhammad M. Qazilbash,[†] Wan Ki Bae,[†] Richard D. Schaller,[†,‡] Jeffrey M. Pietryga,[†] Martin J. Stevens,[§] Burm Baek,[§] Sae Woo Nam,[§] and Victor I. Klimov[†,*]

[†]Center for Advanced Solar Photophysics, Los Alamos National Laboratory, Los Alamos, New Mexico 87545, United States, [‡]Center for Nanoscale Materials, Argonne National Laboratory, Argonne, Illinois 60439, United States, and [§]National Institute of Standards and Technology, Boulder, Colorado 80305, United States

Colloidal semiconductor nanocrystal quantum dots (NQDs) have been studied extensively over the past several years as tunable, low-cost materials for various optoelectronic applications such as light-emitting diodes, lasers, photodetectors, and solar photovoltaics (PV).[1−6] A process observed in NQDs with the potential to impact PV efficiency is carrier multiplication (CM) or multiexciton generation (MEG), in which one absorbed photon with more than two band gaps of energy produces multiple electron−hole (e−h) pairs (excitons).[3] Much attention has been devoted to CM theory[7−13] and experimental study of CM in infrared (IR)-emitting NQDs made of PbSe[10,14−19] and PbS.[17,19,20] More recently, there has been specific focus on the relationship between CM yields in NQDs *versus* bulk semiconductors and the related issue of large discrepancies in the reported CM efficiencies for NQD materials. The latest studies indicate that many apparent inconsistencies in earlier CM reports can be ascribed to distortions in the CM signatures that result from uncontrolled photocharging of nanocrystals, and that these effects can be eliminated by stirring or flowing the NQD solution samples.[16,17,21−24] In this way, PbSe NQDs have been shown to exhibit enhanced CM compared to bulk materials if the CM yields are evaluated as a function of photon energy ($\hbar\omega$) normalized by the band gap energy (E_g).[16,22,23] Recent experimental studies of ref 25 indicate that a further increase in the CM efficiency can be obtained using elongated nanocrystals or nanorods (NRs). However, the observed enhancement is still too moderate to significantly improve PV power conversion.[26−28] Therefore, an important current challenge in the CM field is the development of nanostructures in which the CM performance approaches the energy conservation defined limit where quantum efficiency (QE) of photon-to-exciton conversion increases by 100% per each increment in the photon energy of E_g.

ABSTRACT

Carrier multiplication (CM) is the process in which absorption of a single photon produces multiple electron−hole pairs. Here, we evaluate the effect of particle shape on CM efficiency by conducting a comparative study of spherical nanocrystal quantum dots (NQDs) and elongated nanorods (NRs) of PbSe using a time-resolved technique that is based on photon counting in the infrared using a superconducting nanowire single-photon photodetector (SNSPD). Due to its high sensitivity and low noise levels, this technique allows for accurate determination of CM yields, even with the small excitation intensities required for quantitative measurements, and the fairly low emission quantum yields of elongated NR samples. Our measurements indicate an up to ∼60% increase in multi-exciton yields in NRs *versus* NQDs, which is attributed primarily to a decrease in the electron−hole pair creation energy. These findings suggest that shape control is a promising approach for enhancing the CM process. Further, our work demonstrates the effectiveness of the SNSPD technique for the rapid screening of CM performance in infrared nanomaterials.

The search for new highly efficient CM nanomaterials would be greatly facilitated by developing methods for quick and reliable CM performance screening. Traditionally, CM yields are evaluated *via* time-resolved measurements of carrier dynamics using complex spectroscopic techniques such as femtosecond transient absorption (TA)[14] or photoluminescence (PL) up-conversion (uPL).[17,23] In principle, uPL can provide a higher sensitivity compared to TA as applied to CM studies because the PL intensity scales quadratically with the average NQD exciton occupancy, $\langle N \rangle$,[23] while the scaling of the TA signal is linear[14] (for both measurements, we assume that the lowest band-edge NQD states are not saturated). However, uPL measurements, in which the sample emission is frequency mixed in a nonlinear optical crystal with a short gate pulse, are greatly complicated by a fairly low up-conversion efficiency (typically less than 10%) and the relatively low emission rate of the NQDs that limits the total number of PL photons emitted within a short time window defined by the duration of the gate pulse. As a result, a single, low pump fluence uPL CM measurement (*e.g.*, at $\langle N_{ph} \rangle \sim 0.1$, where $\langle N_{ph} \rangle$ is the average number of photons absorbed per NQD per pulse) can require very long averaging times (often more than 10 h) in order to obtain an adequate signal-to-noise ratio (SNR). Since CM yields are derived from measurements at several different pump intensities, the determination of CM efficiency for a *single sample* can take as long as a week. The development of techniques for quicker CM performance screening is thus an important current challenge in the CM field.

A potential alternative to uPL would be time-correlated single-photon counting (TCSPC). Although TCSPC generally has a lower time resolution (typically tens to hundreds of picoseconds), it is much more sensitive because PL photons are detected directly, without the intermediate step of nonlinear frequency conversion. However, TCSPC has not been commonly applied to IR-emitting materials due to the lack of commercially available IR detectors with detection efficiencies, temporal resolution, and noise comparable to the silicon avalanche photodiodes used in the visible spectral range.

An emerging technology for single-photon counting in the IR involves the use of superconducting nanowire single-photon detectors (SNSPD).[29−31] These detectors operate at telecommunication wavelengths (1.3−1.5 μm) with high detection efficiency, low noise, and very good temporal resolution (tens of picoseconds).[32] An SNSPD consists of a meandering thin nanowire (typically $\sim$5 nm thick by <100 nm wide) of niobium nitride (NbN) that is cooled to below its superconducting critical temperature ($T_c \sim 10$ K) and is current biased to 90−95% of its superconducting critical current.[29,32,33] When the nanowire absorbs a photon, the resulting "hot spot" produces a local resistive region and a subsequent voltage pulse in the radio
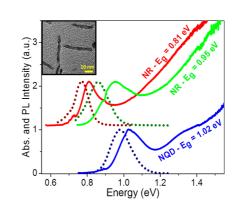

Figure 1. Linear absorption (solid curves) and photolumi-nensence (PL) (dotted) of PbSe NQDs and NRs used in this study; the NR absorption and PL are vertically displaced for clarity. The inset shows a TEM image of the NR sample with $E_g = 0.95$ eV.

frequency electronics. The SNSPDs are usually patterned with about 50% fill factor into a square ($\sim$10 μm by $\sim$10 μm) that is aligned with the core of a single mode optical fiber. System detection efficiencies above 50% at IR wavelengths have been reported, along with low dark count rates ($\sim$100 Hz), no after pulsing, and low timing jitter ($\sim$30 ps).[31,32,34−36] One recent measurement showed the utility of SNSPDs for characterizing the statistical properties of PL emission from a single PbS/CdS nanocrystal at a wavelength of $\sim$1100 nm.[37]

Here, we report the use of an SNSPD in TCSPC studies of multi- and single-exciton dynamics, as well as CM efficiencies in colloidal spherical PbSe NQDs and elongated PbSe NRs. Our results show that the multi-exciton yields in NRs are higher than in spherical NQDs (when compared at the same $\hbar\omega/E_g$), which we attribute to the reduction in the e−h pair creation energy (ε_{eh}), defined as the energy increment necessary for the creation of a new exciton above the CM threshold. Importantly, the use of SNSPDs enables the accurate determination of CM yields 10−100 times *faster* than with a traditional uPL method. Furthermore, using the SNSPD, we obtain measurements of the fast multi-exciton ($\sim$50 ps) and long-lived single-exciton ($\sim$1 μs) dynamics simultaneously. Finally, we find that this new technique is uniquely valuable for studying CM in PbSe NRs, which typically have a lower emission rate, a broader emission spectrum, and a less clearly defined 1S peak as compared to the NQDs,[38] all of which make it difficult to measure CM yields *via* uPL or TA. This demonstrates that this novel technique can serve as a powerful rapid screening tool of the CM performance in IR nanomaterials.

RESULTS AND DISCUSSION

Auger Decay Measurements with SNSPD: Accounting for the Early Time Signal Convolution. In this study, we use oleic-acid-capped PbSe NQDs with a mean radius of 1.8 nm prepared as described previously;[39,40] they exhibit a 1S absorption peak at 1.02 eV (Figure 1, lower absorption
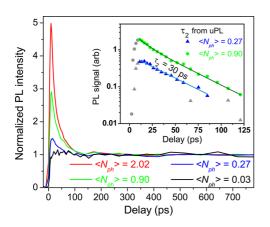
Figure 2. PL dynamics measured *via* uPL for the PbSe NQD sample (E_g = 1.02 eV) excited at 1.55 eV. The low-fluence scan at $\langle N_{ph} \rangle$ = 0.03 (black) shows flat dynamics, suggesting negligible contribution from surface trapping. Inset: Biexciton dynamics extracted from two intermediate-fluence measurements.

spectrum). PbSe NR samples were synthesized through oriented attachment as described in the literature[38,41] and demonstrate relatively narrow 1S absorption features and PL spectra, as shown in Figure 1 (upper spectra). The two PbSe NR samples used in this study had 1S absorption peaks at 0.95 eV (emission at 0.86 eV) and 0.81 eV (emission at 0.765 eV). Mean aspect ratios of 6.9, L = 20.6 nm, and d = 3.0 nm (E_g = 0.95 eV) and 8.4, L = 30.4 nm, and d = 3.6 nm (E_g = 0.81 eV) were determined by transmission electron microscopy (TEM, Figure 1 inset); L is the NR length, and d its diameter.

We first conduct uPL measurements to study the PbSe NQD sample with E_g = 1.02 eV under 1.55 eV excitation for different excitation fluences to obtain multiexciton dynamics and measure the biexciton Auger lifetime (Figure 2). The uPL traces are normalized at times >200 ps, where all transients show essentially flat dynamics, typical for single excitons in the absence of significant surface trapping. Since the photon energy used in these measurements is less than the CM threshold ($E_{th} \sim 2.5-3E_g$),[16,20,23,42] only single excitons are generated in excited NQDs at low fluences. The higher-fluence traces exhibit fast initial decay due to Auger recombination of multiexcitons formed by absorption of multiple photons according to Poissonian statistics, followed by the long-lived single-exciton component. The inset in Figure 2 shows the multi-exction Auger decay of the traces on a semilog scale for two moderate fluences ($\langle N_{ph} \rangle$ = 0.27 and 0.9) obtained by subtracting the long-time single-exciton dynamics.[43] From the fittings, the biexciton Auger lifetime, τ_2, is found to be 30 ps (the trace measured at $\langle N_{ph} \rangle$ = 0.9 also exhibits a weak faster initial component, which is due to triexcitons).

Next, we repeat these measurements with the SNSPD for the same NQD sample (Figure 3a). Again, flat dynamics are observed at low pump fluence for time delays near ~1 ns. At longer times (up to ~0.5 μs),

we observe a single exponential decay with a ~1 μs lifetime (inset of Figure 3a), which can be attributed to recombination of single excitons. The 58 ps instrument response function (IRF) of the SNSPD (Figure 3b inset) is more than an order of magnitude longer than the ~3 ps gate pulse width dominated IRF of the uPL system.[23] Thus, in the SNSPD measurements, the early-time fast PL dynamics are convolved with this 58 ps Gaussian, which necessarily decreases the amplitude of the fast, multi-exciton Auger component and increases the apparent decay time. This effect can be seen in Figure 3c, where we compare simulated traces from uPL and the SNSPD with similar Auger decay time constants.

As discussed previously in the literature, the CM yields are usually derived from TA or PL time transient measured at low pump fluences ($\langle N_{ph} \rangle \ll 1$). Specifically, QE of photon-to-exciton conversion can be determined from the ratio of the early-time signal amplitude before Auger recombination (A) and the amplitude of a late-time single-exciton signal (B).[14,23] In order to apply this procedure to the SNSPD data, we must first correct for the "amplitude loss" of the fast initial PL component associated with multiexciton decay. In order to make this correction, we obtain accurate Auger recombination lifetimes from the higher temporal resolution uPL measurements as described above.

Knowing the IRF of the SNSPD and the sample biexciton Auger lifetime, it is possible to accurately derive the "true" A/B ratios from the convolved (raw) values measured by the SNSPD. To obtain the correction factors for the A/B ratios, we use simulated PL dynamics with a short rise time defined by the duration of the pump pulse followed by fast exponential Auger decay (tens to hundreds of picoseconds) and then a slower single-exciton signal described either by a constant (in the case of short subnanosecond scans) or one- or two-exponential decay (in the case of longer, microsecond scans). To simulate the corresponding SNSPD traces ($PL_{SNSPD}(t)$), the PL dynamics ($PL(t)$) are numerically convolved with the IRF:

$$PL_{SNSPD}(t) = \int_{-\infty}^{\infty} PL(\tau) \times IRF(t - \tau)d\tau$$

In Figure 3d, we illustrate this procedure for the sample with the 30 ps biexciton Auger lifetime using the 3 and 58 ps Gaussian IRFs for uPL and SNSPD measurements, respectively. The comparison of the calculated (lines) and the measured (symbols) traces indicates that this model accurately reproduces both signal amplitudes and temporal dynamics in the case of both uPL and SNSPD measurements. The inset of Figure 3d compares the corrected A/B ratio from the SNSPD with the A/B ratio from uPL, showing good agreement of the obtained values.

In Figure 3c, we apply the convolution procedure to several simulated PL traces with different τ_2 constants and the same A/B ratio of 2. As expected, a decrease in
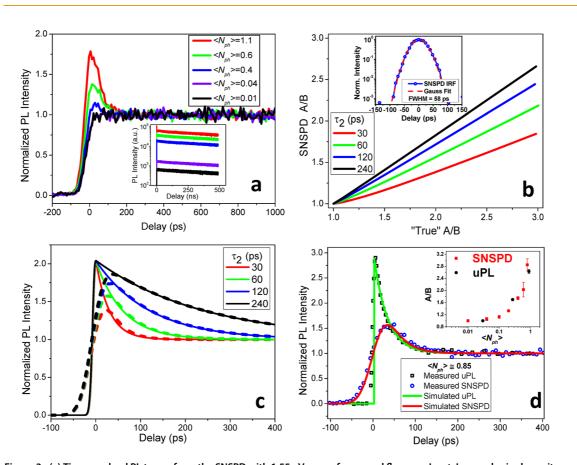
Figure 3. (a) Time-resolved PL traces from the SNSPD with 1.55 eV pump for several fluences. Inset: Log-scale single-exciton dynamics taken simultaneously with the short-time multiexciton dynamics. (b) Dependence of the apparent A/B ratio (measured by SNSPD) on the "true" A/B ratio (obtained *via* deconvolution) for different τ_2 (indicated in the legend) and IRF of 58 ps. Note that if $\tau_2 \sim 200$ ps, the correction due to deconvolution is less than 10%. Inset: 58 ps instrument response function (IRF) of SNSPD fitted to a Gaussian profile. (c) Simulated PL dynamics from uPL (solid lines) and SNSPD (dashed lines) for several biexciton Auger decay times (τ_2; indicated in the legend) and for an IRF of 58 ps. (d) Two PL traces for similar pump fluence measured with uPL (black squares) and SNSPD (blue circles) showing the effect of the Gaussian IRF convolution. Also shown are simulated dynamics for uPL (green line) and for the SNSPD (red line); see text for details. Inset: Corrected A/B ratio from SNSPD (from panel a) compared to the A/B ratio obtained *via* uPL (from Figure 2).

the Auger lifetime leads to a more substantial loss of the initial fast component in the convolved traces. We further notice that, for Auger decay times greater than the IRF width, the relationship between the "true" and convolved (raw) A/B ratios is nearly linear (Figure 3b). However, for Auger lifetimes on the order of the IRF width or shorter, the dependence becomes increasingly nonlinear (see Supporting Information for additional details on the deconvolution procedure).

While the effect of signal convolution is undesirable, particularly when studying samples with short biexciton Auger lifetimes, the utility of the SNSPD is apparent when one considers the time required to acquire low-fluence measurements with uPL *versus* the SNSPD. For example, the uPL measurements for pump fluence of 6×10^{13} photons/cm^{-2} per pulse shown in Figure 2 required more than 10 h to record and produced a SNR of $\sim$19 (13 counts/s average with 0.69 count/s standard deviation on the long-time single-exciton dynamics). On the other hand, the SNSPD measurements with *half the fluence* (3×10^{13} photons/cm^2 per pulse, Figure 3a) took only 5 min and

produced a SNR of 33.4 (1721 counts/s average with standard deviation of 51.5 count/s). In addition to decreased measurement times and the increased SNR, the use of the SNSPD allows us to accumulate a much greater amount of data per single trace, which increases the accuracy of fitting procedures. For example, in the uPL measurements, we usually acquire only $\sim$50 data points spaced logarithmically in time to increase the number of points during the initial Auger decay. This approach allows for a more accurate determination of the Auger lifetime; however, it reduces the amount of data describing long-time dynamics. For example, typically, we have only *ca.* 10 data points between 300 ps and 1 ns. In the SNSPD measurements, however, the bins are linearly spaced by 8 ps throughout the entire trace, producing 125 data points for the 1 ns scan of interest without a bias against either short- or long-time dynamics. Furthermore, the timing system histogram has 65 536 time bins, so with 8 ps bins, we simultaneously record PL dynamics at times up to $\sim$650 ns.

SNSPD Measurements of CM in PbSe Nanorods. In order to test the applicability of the SNSPD to CM studies, we
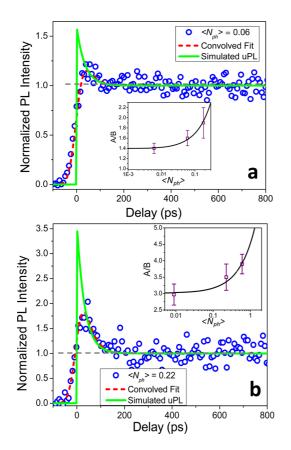
Figure 4. Low-fluence PL dynamics measured with the SNSPD for the PbSe NQD samples excited at (a) 3.1 eV and (b) 4.65 eV. The insets show the extrapolation of the A/B ratios to the zero-fluence limit to obtain the CM yields. The values used in the inset are obtained from the deconvolved traces (that is, simulated uPL traces; green lines). The gray dashed line is a "single-exciton scale bar".

first use this system to measure PL dynamics for the same 1.02 eV band gap PbSe NQD sample under excitation at energies at which measurable CM is expected. Figure 4 shows low pump fluence traces (circles) acquired with 3.1 eV (a) and 4.65 eV (b) pump photon energies, fits to the experimental data (dashed red lines), and traces obtained from these fits through deconvolution (solid green lines) using the measured IRF and the 30 ps biexciton Auger lifetime derived *via* uPL. From a linear extrapolation (lines in the insets of Figure 4) of the corrected A/B ratios measured for different pump intensities (symbols in the insets of Figure 4), we find that in the limit $\langle N_{\mathrm{ph}} \rangle \to 0$, A/B is 1.4 and 3.0 for the 3.1 and 4.65 eV photon energies, respectively. Using the expression QE = $(A/B + 2)/3$,[16] we can then obtain QE of 1.18 ± 0.03 for 3.1 eV and 1.65 ± 0.03 for 4.65 eV. The corresponding multiexciton yields ($\eta = $ QE $- 1$) are 0.18 and 0.65. These values are in good agreement with previously reported CM efficiencies for spherical PbSe NQDs measured *via* traditional TA and uPL techniques.[16,22,23]

Next, we proceed to CM measurements of PbSe NRs. For the NR studies, a NbTiN SNSPD device fabricated by Jet Propulsion Laboratory was used and showed an improved IRF of 48 ps. In Figure 5, we show PL dynamics for the NR sample with $E_{\mathrm{g}} = 0.95$ eV measured with the SNSPD (a) and uPL (b) using excitation at 1.55 eV. For this excitation energy, CM is not energetically possible and multiexcitons can be generated only at high fluences *via* absorption of multiple photons from the same pulse. We use these measurements to quantify the biexciton Auger lifetime.
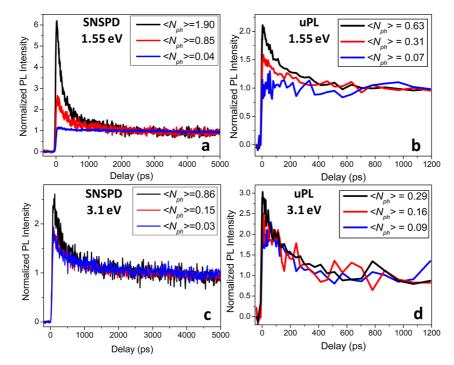

Figure 5. PL dynamics for the PbSe NR sample ($E_{\mathrm{g}} = 0.95$ eV) measured with SNSPD (a,c) and uPL (b,d) using excitation at 1.55 eV (a,b) and 3.1 eV (c,d). From the 3.1 eV data, $\eta = 0.29$ for the SNSPD measurement and $\eta = 0.27$ for the uPL measurement.
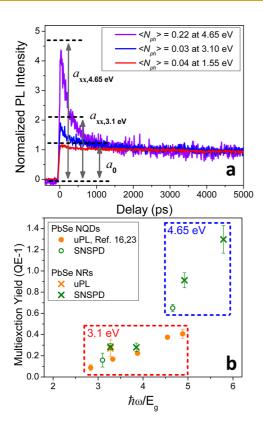
Figure 6. (a) Comparison of the low-fluence SNSPD measurements with excitation at 1.55, 3.1, and 4.65 eV for the NR sample with E_g = 0.95 eV; a_{xx} amplitudes shown in the plot account for deconvolution. (b) Summary of the CM results for the PbSe NRs (crosses; present work) and NQDs (circles) from both the present work (open green circles) and refs 16 and 23 (closed orange circles) obtained for two excitation energies: 3.1 and 4.65 eV. Note that the SNSPD and uPL data points measured for NRs at $\hbar\omega/E_g$ = 3.28 overlap with each other.

One can see that even after a ~10 h scan, the lowest-fluence single-excitonic uPL signal is quite noisy due to low emission rates typical of NR samples. Also, because of a high noise level and a limited temporal range (<1.2 ns), uPL does not allow us to infer any slow single-exciton time constants. On the other hand, in addition to a much higher SNR, the SNSPD measurements clearly reveal slow multiexponential dynamics that reflect single-exciton relaxation. Specifically, we can extract characteristic time constants of 2.5–5 and ~250 ns that are not resolvable with uPL. From the uPL and SNSPD traces, we obtained Auger recombination lifetimes for NR samples of $\tau_2 = 220 \pm$ 40 ps (E_g = 0.95 eV) and 392 $\pm$ 42 ps (E_g = 0.81 eV). These values are longer than those of spherical NQDs with the same E_g, which is consistent with the volume-dependent scaling of Auger decay time constants.[44]

PL dynamics measured for 3.1 eV excitation are shown in Figure 5c (SNSPD) and 5d (uPL). Also, SNSPD-measured dynamics using 4.65 eV excitation appear in Figure 6a. In the case of the 3.1 eV photon energy, the unprecedented sensitivity of the SNSPD allows for a more accurate quantification of CM yields by using extremely low pump fluences ($\langle N_{ph} \rangle \approx 0.03$). Both the lowest-fluence SNSPD and uPL traces (blue curves in Figure 5c,d) were

acquired using 10−12 h averaging. The comparison of these data again demonstrates a much lower noise level for the SNSPD detection compared to uPL. Additionally, with the SNSPD, we were able to measure the PL dynamics and the CM yield of the NR samples with excitation at 4.65 eV (Figure 6a), which was not possible with the uPL system because of insufficient signal level.

As mentioned earlier, the PbSe NRs in this study exhibit more complicated PL dynamics in comparison to NQDs. Specifically, the 2.5 ns decay component is present even for low-fluence excitation at 1.55 eV. Its magnitude does not depend on pump intensity, suggesting that it is not due to Auger recombination but instead arises possibly from trapping at surface defects (see Figure 6a). In order to correct for these trapping dynamics, we follow a previously described procedure.[45] Briefly, we first correct the A/B ratios of the low-fluence 1.55 eV pump traces for the SNSPD IRF convolution; since the 2.5 ns decay is much longer than the IRF width, this correction is negligible. Next, we extrapolate initial A/B values to zero fluence, which produces the "trapping" correction factor $a_0 = A_0/B_0$ (Figure 6a). We then normalize the low-pump-intensity $a_{xx} = A/B$ ratios, derived in the usual way for the 3.1 or 4.65 eV pump photon energies, by a_0 and use these values to determine CM efficiencies: QE = $(a_{xx}/a_0 + 2)/3$.

The CM yields, η, obtained in this way for the NRs are shown in Figure 6b (crosses) together with a collection of data for spherical PbSe NQDs (circles) that includes both present SNSPD measurements and literature uPL results.[16,23] For the NR sample with E_g = 0.95 eV, we also show a data point obtained via uPL in order to compare it with the SNSPD result. The excellent agreement between the two measurements reinforces the validity of the new measurement technique.

Comparing the CM results for PbSe NRs with their spherical counterparts, we can see that, at the same $\hbar\omega/E_g$, the NRs show an enhancement of the CM yield (by ca. 30−60% for the samples studied here) over NQDs. From the data in Figure 6b, we can also estimate the e−h pair creation energy. In the literature, ε_{eh} is often derived from the CM data obtained for the same excitation energy but for differently sized samples using the slope of the η versus $\hbar\omega/E_g$ dependence ($\hbar\omega$ is fixed; E_g varies). However, a rigorous determination of this value would require that measurements be done on the same sample for a series of different photon energies (E_g is fixed; $\hbar\omega$ varies). Using the data points obtained with excitation at 3.1 and 4.65 eV, we can estimate ε_{eh} for the NRs. Specifically, on the basis of CM yields measured for the sample with E_g = 0.81 eV, we obtain ε_{eh} of ~$2.6E_g$. For comparison, the NQDs with a similar energy gap (E_g = 1 eV) studied in this work show ε_{eh} of approximately $3.2E_g$. This suggests that the observed enhancement of CM in NRs versus NQDs is primarily due to the reduction of the e−h pair creation energy.

While our results demonstrate an increase in CM yields for NRs as compared to the spherical NQDs, the

observed enhancement is lower than that in the recently published study by Cunnigham et al.[25] The exact reasons for this discrepancy are still not clear. However, we would like to point out that the NRs studied here are longer (aspect ratios 7−8) than the ones investigated in ref 25 (aspect ratio ∼4), and the effects of this parameter are still under investigation. Another possibility is a potential effect of photocharging that might have affected the CM measurements in ref 25. The authors did stir their samples to prevent accumulation of charged NRs within the excitation volume. However, in some of our measurements, we noticed that even in stirred samples, NRs tend to form a deposit (a thin film) on the inner side of the entrance wall of the optical cuvette, which is usually accompanied by an increase in the apparent A/B ratio due to photocharging in the NRs localized within the deposit. This type of photoinduced film deposit, previously observed in other NR systems,[46] is probably due to photoionization and is more pronounced for UV excitation. To avoid this in the samples that were prone to form a deposit, we continuously moved them with a micrometer-driven optical stage during the measurements in addition to stirring. This allowed us to obtain highly reproducible results, while the reproducibility was fairly poor when the samples prone to depositing were not moved. We noticed that this problem seems characteristic of the NR samples only; the NQD samples were not especially prone to forming the deposit during photoexcitation.

The effects of photocharging in NR samples are illustrated in Figure S2 of Supporting Information, where we compare the PL traces taken for the same sample under two different conditions: in one case, the sample is stirred, and in the other case, in addition to stirring, the sample is simultaneously translated during the measurements to avoid sample deposition on the walls of the cuvette. The sample, which was only stirred but not translated, shows typical signatures of photocharging, that is, a much higher "apparent" CM yield[16] and a faster initial Auger decay. These artifacts are removed if the sample is translated, which allows for accurate determination of the CM yields and neutral biexciton Auger lifetimes.

Due to the slower Auger recombination observed in NRs, the observed enhancement of CM seems to be counterintuitive since both processes are described by the same matrix element. While at present we do not have a definite explanation of this trend, we can suggest a few possible reasons for the observed increased in CM yields in the NRs. First, we would like to point out that, in addition to the Coulomb interaction matrix element, the rates of CM (r_{CM}) and Auger decay (r_A) depend on

densities of states of final states—biexcitons (g_2) in the CM case and high-energy single excitons (g_1) in the case of Auger recombination. If one accounts for the density of state factors, the rates of these processes can be related by $r_{CM} \propto (g_2/g_1)r_{2A}$.[20] One might expect that in the NR samples the ratio of g_2 and g_1 is greater than in the quantum dots because of, for example, symmetry breaking accompanied by the increase in the number of biexciton states accessible in the course of the CM process. An additional factor is a possible aspect-ratio-dependent rate of intraband cooling processes competing with CM. For example, there are indications that the carrier−phonon coupling is reduced in NRs compared to quantum dots.[47,48] Further, one might expect that the rate of carrier cooling via Coulombic processes such as Auger-type e−h energy transfer[49,50] is also reduced upon elongation. Both of these effects would favor CM in the competition between this process and alternative energy loss mechanisms.

CONCLUSIONS

In conclusion, we have used a traditional uPL technique and a photon counting method with SNSPDs to conduct comparative side-by-side studies of multiexciton dynamics and CM in spherical (NQDs) and elongated (NRs) nanocrystals of PbSe. These studies reveal an increase in the CM efficiency in the NRs compared to the NQDs, which occurs primarily due to a reduction in the e−h pair creation energy. Specifically, the measurements of samples with a similar energy gap (0.8−1 eV) indicate ε_{eh} of ∼2.6E_g in NRs versus ∼3.2E_g in NQDs. Importantly, both of these values are significantly lower than ε_{eh} in bulk PbSe (∼5E_g)[51] if expressed in terms of E_g.

This work demonstrates the significant promise of SNSPDs for quick screening of the CM performance of IR nanomaterials. Specifically, we show that we can accurately correct for the early-time PL amplitude convolution due to SNDPD IRF limitations by using Auger lifetimes derived from fairly straightforward uPL measurements of biexciton dynamics. Also, we demonstrate that SNSPDs allow for 10−100 times higher PL count rates and a greatly improved SNR compared to uPL. This is especially important in the case of the low pump fluences required in CM measurements. Furthermore, the SNSPD provides both fast multiexciton (<100 ps) and long single-exciton (∼microseconds) dynamics simultaneously. We believe that the use of SNSPDs, which allows for quick measurements of PL dynamics in IR-emitting nanostructures at extremely low signal levels, can greatly facilitate the search for new, more efficient CM materials for application in future solar cell technologies.

EXPERIMENTAL SECTION

For spectroscopy, all samples are dispersed in hexane in an inert atmosphere glovebox and loaded into 1 mm path

length air-free cuvettes, maintaining the 1S absorption optical density below 0.1. During spectroscopic measurements, the samples were stirred vigorously to avoid any

distortion of multiexciton dynamics and CM results from photocharging.[16,20,21,23]

Carrier recombination dynamics were studied by monitoring PL decay upon excitation by ~1 ps (fwhm) pulses from a 250 kHz amplified Ti:sapphire laser at either the fundamental wavelength (1.55 eV), the second (3.1 eV), or the third (4.65 eV) harmonic. The PL decay was measured with both the uPL and the SNSPD systems. In the uPL measurements, the sum-frequency signal was generated by mixing the laser fundamental radiation with NQD emission in a nonlinear crystal of a β-barium borate. The sum-frequency signal was then spectrally filtered with a monochromator (bandwidth ~50 meV centered around the PL emission peak) and detected by a photomultiplier tube.

In the SNSPD measurements, the sample emission was spectrally filtered with a monochromator and then coupled into an optical fiber delivering the PL signal to the SNSPD housed in a closed-loop helium cryo-cooler system.[36] The NbN SNSPD was kept at ~3.5 K with ~0.02 K temperature fluctuations and biased to ~90% of its superconducting critical current (typically ~20 μA). The voltage pulses were amplified and read out with a Picoquant Hydraharp. Typically, 8 ps timing bins were used in these studies. Two different devices were used in these measurements. For the NQD studies, a NbN device fabricated at Massachusetts Institute of Technology (MIT) and MIT Lincoln Laboratory was used, which exhibited a Gaussian instrument response function (IRF) with a 58 ps width limited primarily by the electronic timing jitter. A NbTiN nanowire device fabricated by Jet Propulsion Laboratory was used for the NRs studies and showed a IRF of 48 ps. All of the devices were packaged at the National Institute of Standards and Technology (NIST) in Boulder, Colorado.

REFERENCES AND NOTES

1. Klimov, V. I. *Nanocrystal Quantum Dots*; 2nd ed.; CRC Press: Boca Raton, FL, 2010.
2. Kim, T.-H.; Cho, K.-S.; Lee, E. K.; Lee, S. J.; Chae, J.; Kim, J. W.; Kim, D. H.; Kwon, J.-Y.; Amaratunga, G.; Lee, S. Y.; Choi, B. L.; Kuk, Y.; Kim, J. M.; Kim, K. Full-Colour Quantum Dot Displays Fabricated by Transfer Printing. *Nat. Photonics* **2011**, *5*, 176–182.
3. Semonin, O. E.; Luther, J. M.; Choi, S.; Chen, H.-Y.; Gao, J.; Nozik, A. J.; Beard, M. C. Peak External Photocurrent Quantum Efficiency Exceeding 100% *via* MEG in a Quantum Dot Solar Cell. *Science* **2011**, *334*, 1530–1533.
4. Sargent, E. H. Colloidal Quantum Dot Solar Cells. *Nat. Photonics* **2012**, *6*, 133–135.
5. Klimov, V. I.; Mikhailovsky, A. A.; Xu, S.; Malko, A.; Hollingsworth, J. A.; Leatherdale, C. A.; Eisler, H.-J.; Bawendi, M. G. Optical Gain and Stimulated Emission in Nanocrystal Quantum Dots. *Science* **2000**, *290*, 314–317.
6. Caruge, J. M.; Halpert, J. E.; Wood, V.; Bulovic, V.; Bawendi, M. G. Colloidal Quantum-Dot Light-Emitting Diodes with Metal-Oxide Charge Transport Layers. *Nat. Photonics* **2008**, *2*, 247–250.
7. Califano, M.; Zunger, A.; Franceschetti, A. Direct carrier multiplication due to inverse Auger scattering in CdSe quantum dots. *Appl. Phys. Lett.* **2004**, *84*, 2409–2411.
8. Rabani, E.; Baer, R. Theory of Multiexciton Generation in Semiconductor Nanocrystals. *Chem. Phys. Lett.* **2010**, *496*, 227–235.
9. Rupasov, V. I.; Klimov, V. I. Carrier multiplication in semiconductor nanocrystals via intraband optical transitions involving virtual biexciton states. *Phys. Rev. B* **2007**, *76*, 125321.
10. Allan, G.; Delerue, C. Influence of Electronic Structure and Multiexciton Spectral Density on Multiple-Exciton Generation in Semiconductor Nanocrystals: Tight-Binding Calculations. *Phys. Rev. B* **2008**, *77*, 125340.
11. Isborn, C. M.; Kilina, S. V.; Li, X.; Prezhdo, O. V. Generation of Multiple Excitons in PbSe and CdSe Quantum Dots by Direct Photoexcitation: First-Principles Calculations on Small PbSe and CdSe Clusters. *J. Phys. Chem. C* **2008**, *112*, 18291–18294.
12. Lin, Z.; Franceschetti, A.; Lusk, M. T. Size Dependence of the Multiple Exciton Generation Rate in CdSe Quantum Dots. *ACS Nano* **2011**, *5*, 2503–2511.
13. Witzel, W. M.; Shabaev, A.; Hellberg, C. S.; Jacobs, V. L.; Efros, A. L. Quantum Simulation of Multiple-Exciton Generation in a Nanocrystal by a Single Photon. *Phys. Rev. Lett.* **2010**, *105*, 137401.
14. Schaller, R. D.; Klimov, V. I. High Efficiency Carrier Multiplication in PbSe Nanocrystals: Implications for Solar Energy Conversion. *Phys. Rev. Lett.* **2004**, *92*, 186601.
15. Ellingson, R. J.; Beard, M. C.; Johnson, J. C.; Yu, P.; Micic, O. I.; Nozik, A. J.; Shabaev, A.; Efros, A. L. Highly Efficient Multiple Exciton Generation in Colloidal PbSe and PbS Quantum Dots. *Nano Lett.* **2005**, *5*, 865–871.
16. McGuire, J. A.; Sykora, M.; Joo, J.; Pietryga, J. M.; Klimov, V. I. Apparent *versus* True Carrier Multiplication Yields in Semiconductor Nanocrystals. *Nano Lett.* **2010**, *10*, 2049–2057.
17. Nair, G.; Geyer, S. M.; Chang, L.-Y.; Bawendi, M. G. Carrier Multiplication Yields in PbS and PbSe Nanocrystals Measured by Transient Photoluminescence. *Phys. Rev. B* **2008**, *78*, 125325.
18. Miaja-Avila, L.; Tritsch, J. R.; Wolcott, A.; Chan, W. L.; Nelson, C. A.; Zhu, X. Y. Direct Mapping of Hot-Electron Relaxation and Multiplication Dynamics in PbSe Quantum Dots. *Nano Lett.* **2012**, *12*, 1588–1591.
19. Gesuele, F.; Sfeir, M. Y.; Koh, W. K.; Murray, C. B.; Heinz, T. F.; Wong, C. W. Ultrafast Supercontinuum Spectroscopy of Carrier Multiplication and Biexcitonic Effects in Excited States of PbS Quantum Dots. *Nano Lett.* **2012**, *12*, 2658–2664.
20. Stewart, J. T.; Padilha, L. A.; Qazilbash, M. M.; Pietryga, J. M.; Midgett, A. G.; Luther, J. M.; Beard, M. C.; Nozik, A. J.; Klimov, V. I. Comparison of Carrier Multiplication Yields in PbS and PbSe Nanocrystals: The Role of Competing Energy-Loss Processes. *Nano Lett.* **2012**, *12*, 622–628.
21. McGuire, J. A.; Sykora, M.; Robel, I.; Padilha, L. A.; Joo, J.; Pietryga, J. M.; Klimov, V. I. Spectroscopic Signatures of Photocharging due to Hot-Carrier Transfer in Solutions of Semiconductor Nanocrystals under Low-Intensity Ultraviolet Excitation. *ACS Nano* **2010**, *4*, 6087–6097.
22. Midgett, A. G.; Hillhouse, H. W.; Hughes, B. K.; Nozik, A. J.; Beard, M. C. Flowing *versus* Static Conditions for Measuring Multiple Exciton Generation in PbSe Quantum Dots. *J. Phys. Chem. C* **2010**, *114*, 17486–17500.
23. McGuire, J. A.; Joo, J.; Pietryga, J. M.; Schaller, R. D.; Klimov, V. I. New Aspects of Carrier Multiplication in Semiconductor Nanocrystals. *Acc. Chem. Res.* **2008**, *41*, 1810–1819.
24. Padilha, L. A.; Robel, I.; Lee, D. C.; Nagpal, P.; Pietryga, J. M.; Klimov, V. I. Spectral Dependence of Nanocrystal Photoionization Probability: The Role of Hot-Carrier Transfer. *ACS Nano* **2011**, *5*, 5045–5055.
25. Cunningham, P. D.; Boercker, J. E.; Foos, E. E.; Lumb, M. P.; Smith, A. R.; Tischler, J. G.; Melinger, J. S. Enhanced Multiple Exciton Generation in Quasi-One-Dimensional Semiconductors. *Nano Lett.* **2011**, *11*, 3476–3481.
26. Klimov, V. I. Detailed-Balance Power Conversion Limits of Nanocrystal-Quantum-Dot Solar Cells in the Presence of Carrier Multiplication. *Appl. Phys. Lett.* **2006**, *89*, 123118.

27. Beard, M. C.; Midgett, A. G.; Law, M.; Semonin, O. E.; Ellingson, R. J.; Nozik, A. J. Variations in the Quantum Efficiency of Multiple Exciton Generation for a Series of Chemically Treated PbSe Nanocrystal Films. *Nano Lett.* **2009**, *9*, 836–845.

28. Hanna, M. C.; Nozik, A. J. Solar Conversion Efficiency of Photovoltaic and Photoelectrolysis Cells with Carrier Multiplication Absorbers. *J. Appl. Phys.* **2006**, *100*, 074510–074518.

29. Gol'tsman, G. N.; Okunev, O.; Chulkova, G.; Lipatov, A.; Semenov, A.; Smirnov, K.; Voronov, B.; Dzardanov, A.; Williams, C.; Sobolewski, R. Picosecond Superconducting Single-Photon Optical Detector. *Appl. Phys. Lett.* **2001**, *79*, 705–707.

30. Hadfield, R. H. Single-Photon Detectors for Optical Quantum Information Applications. *Nat. Photonics* **2009**, *3*, 696–705.

31. Natarajan, C. M.; Tanner, M. G.; Hadfield, R. H. Superconducting Nanowire Single-Photon Detectors: Physics and Applications. *Supercond. Sci. Technol.* **2012**, *25*, 063001.

32. Gol'tsman, G.; Minaeva, O.; Korneev, A.; Tarkhov, M.; Rubtsova, I.; Divochiy, A.; Milostnaya, I.; Chulkova, G.; Kaurova, N.; Voronov, B. Middle-Infrared to Visible-Light Ultrafast Superconducting Single-Photon Detectors. *IEEE Trans. Appl. Supercond.* **2007**, *17*, 246.

33. Verevkin, A.; Pearlman, A.; Slysz, W.; Zhang, J.; Currier, M.; Korneev, A.; Chulkova, G.; Okunev, O.; Kouminov, P.; Smirnov, K.; Voronov, B.; Gol'tsman, G. N.; Sobolewski, R. Ultrafast Superconducting Single-Photon Detectors for Near-Infrared-Wavelength Quantum Communications. *J. Mod. Opt.* **2004**, *51*, 1447–1458.

34. Divochiy, A.; Marsili, F.; Bitauld, D.; Gaggero, A.; Leoni, R.; Mattioli, F.; Korneev, A.; Seleznev, V.; Kaurova, N.; Minaeva, O.; Gol'tsman, G.; Lagoudakis, K. G.; Benkhaoul, M.; Levy, F.; Fiore, A. Superconducting Nanowire Photon-Number-Resolving Detector at Telecommunication Wavelengths. *Nat. Photonics* **2008**, *2*, 302–306.

35. Rosfjord, K. M.; Yang, J. K. W.; Dauler, E. A.; Kerman, A. J.; Anant, V.; Voronov, B. M.; Gol'tsman, G. N.; Berggren, K. K. Nanowire Single-Photon Detector with an Integrated Optical Cavity and Anti-Reflection Coating. *Opt. Express* **2006**, *14*, 527–534.

36. Stevens, M. J.; Hadfield, R. H.; Schwall, R. E.; Nam, S. W.; Mirin, R. P.; Gupta, J. A. Fast Lifetime Measurements of Infrared Emitters Using a Low-Jitter Superconducting Single-Photon Detector. *Appl. Phys. Lett.* **2006**, *89*, 031109.

37. Correa, R. E.; Dauler, E. A.; Nair, G.; Pan, S. H.; Rosenberg, D.; Kerman, A. J.; Molnar, R. J.; Hu, X.; Marsili, F.; Anant, V.; Berggren, K. K.; Bawendi, M. G. Single Photon Counting from Individual Nanocrystals in the Infrared. *Nano Lett.* **2012**, *12*, 2953–2958.

38. Bartnik, A. C.; Efros, A. L.; Koh, W. K.; Murray, C. B.; Wise, F. W. Electronic States and Optical Properties of PbSe Nanorods and Nanowires. *Phys. Rev. B* **2010**, *82*, 195313.

39. Pietryga, J. M.; Werder, D. J.; Williams, D. J.; Casson, J. L.; Schaller, R. D.; Klimov, V. I.; Hollingsworth, J. A. Utilizing the Lability of Lead Selenide To Produce Heterostructured Nanocrystals with Bright, Stable Infrared Emission. *J. Am. Chem. Soc.* **2008**, *130*, 4879–4885.

40. Joo, J.; Pietryga, J. M.; McGuire, J. A.; Jeon, S.-H.; Williams, D. J.; Wang, H.-L.; Klimov, V. I. A Reduction Pathway in the Synthesis of PbSe Nanocrystal Quantum Dots. *J. Am. Chem. Soc.* **2009**, *131*, 10620–10628.

41. Koh, W.-k.; Bartnik, A. C.; Wise, F. W.; Murray, C. B. Synthesis of Monodisperse PbSe Nanorods: A Case for Oriented Attachment. *J. Am. Chem. Soc.* **2010**, *132*, 3909–3913.

42. Beard, M. C.; Midgett, A. G.; Hanna, M. C.; Luther, J. M.; Hughes, B. K.; Nozik, A. J. Comparing Multiple Exciton Generation in Quantum Dots To Impact Ionization in Bulk Semiconductors: Implications for Enhancement of Solar Energy Conversion. *Nano Lett.* **2010**, *10*, 3019–3027.

43. Klimov, V. I.; Mikhailovsky, A. A.; McBranch, D. W.; Leatherdale, C. A.; Bawendi, M. G. Quantization of Multiparticle Auger Rates in Semiconductor Quantum Dots. *Science* **2000**, *287*, 1011–1013.

44. Robel, I.; Gresback, R.; Kortshagen, U.; Schaller, R. D.; Klimov, V. I. Universal Size-Dependent Trend in Auger Recombination in Direct-Gap and Indirect-Gap Semiconductor Nanocrystals. *Phys. Rev. Lett.* **2009**, *102*, 177404.

45. Schaller, R. D.; Sykora, M.; Jeong, S.; Klimov, V. I. High-Efficiency Carrier Multiplication and Ultrafast Charge Separation in Semiconductor Nanocrystals Studied *via* Time-Resolved Photoluminescence. *J. Phys. Chem. B* **2006**, *110*, 25332–25338.

46. Kazes, M.; Lewis, D. Y.; Banin, U. Method for Preparation of Semiconductor Quantum-Rod Lasers in a Cylindrical Microcavity. *Adv. Funct. Mater.* **2004**, *14*, 957–962.

47. Lange, H.; Mohr, M.; Artemyev, M.; Woggon, U.; Niermann, T.; Thomsen, C. Optical Phonons in Colloidal CdSe Nanorods. *Phys. Status Solidi B* **2010**, *247*, 2488–2497.

48. Kelley, A. M. Electron−Phonon Coupling in CdSe Nanocrystals. *J. Phys. Chem. Lett.* **2010**, *1*, 1296–1300.

49. Efros, A. L.; Kharchenko, V. A.; Rosen, M. Breaking the Phonon Bottleneck in Nanometer Quantum Dots—Role of Auger-like Processes. *Solid State Commun.* **1995**, *93*, 281–284.

50. Wang, L.-W.; Califano, M.; Zunger, A.; Franceschetti, A. Pseudopotential Theory of Auger Processes in CdSe Quantum Dots. *Phys. Rev. Lett.* **2003**, *91*, 056404.

51. Pijpers, J. J. H.; Ulbricht, R.; Tielrooij, K. J.; Osherov, A.; Golan, Y.; Delerue, C.; Allan, G.; Bonn, M. Assessment of Carrier-Multiplication Efficiency in Bulk PbSe and PbS. *Nat. Phys.* **2009**, *5*, 811–814.